5

Silanization with APTES for Controlling the Interactions Between Stainless Steel and Biocomponents: Reality vs Expectation

Jessem Landoulsi[1], Michel J. Genet[2], Karim El Kirat[3], Caroline Richard[4], Sylviane Pulvin[5] and Paul G. Rouxhet[2]
[1]*Laboratoire de Réactivité de Surface, Université Pierre & Marie Curie -Paris VI,*
[2]*Institute of Condensed Matter and Nanosciences – Bio & Soft Matter, Université Catholique de Louvain,*
[3]*Laboratoire de Biomécanique et Bioingénierie,*
[4]*Laboratoire Roberval,*
[5]*Génie Enzymatique et Cellulaire, Université de Technologie de Compiègne,*
[1,3,4,5]*France*
[2]*Belgium*

1. Introduction

The surface of biomaterials is frequently chemically modified with the aim to modify the physicochemical properties (hydrophobicity, electrical charge, solvation) which control the interactions with biomolecules and consequently with cell surfaces, or to retain biochemical entities which are specifically recognized by the cells (Williams, 2010). Regarding inorganic materials, widespread procedures involve self-assembly of alcane thiols on gold, silver, copper or platinum (Wink et al., 1997). However, these substrates have limited interest in biomedical applications. Other procedures consist in grafting organosilanes on silica and other metal oxides (Weetall, 1993). The use of silane coupling agents has been reported in various biomaterials researches, such as surface modification of titanium (Nanci et al., 1998), natural fiber/polymer composites (Xie et al., 2010) or dental ceramics (Matinlinna et al., 2004; Matinlinna & Vallittu, 2007).

The silanization reaction at interfaces is complex and there is still considerable debate on the retention mechanisms and on the organization of the interface (Gooding & Ciampi, 2011; Haensch et al., 2010, Suzuki & Ishida, 1996). Depending on the nature of reactive moieties bound to Si in the silane (typically Cl or alkoxy group) and their number, and on the reaction conditions (particularly the presence of water), the relative importance of covalent binding to the surface, oligomerization, polymerization along the surface plane, three-dimensional polymerization may possibly vary. The efficiency of the surface modification is often demonstrated by its influence on biochemical or biological activity. However the nature of the interface produced is difficult to characterize, which limits the guidelines

available to improve the procedures. Moreover organic contaminants are always present on high energy solids. They are mainly of hydrocarbon nature and are readily adsorbed from surrounding air or in surface analysis spectrometers (Caillou et al., 2008; Landoulsi et al., 2008a). The possible influence of contaminants on the silanization process and product is usually not considered. In the case of silicon wafer silanized with 3-[methoxy(polyethyleneoxy)]propyl trimethoxysilane and trichlorosilane in organic solvents under a controlled atmosphere, the surface obtained was described as a 1 to 2 nm thick grafted silane layer covered by a thin layer of adventitious contaminants, suggesting that contamination was posterior to the silanization reaction. On the other hand, the silane layer was not stable in phosphate buffered saline at 37°C (Dekeyser et al., 2008).

Aminopropylalkoxysilanes are attractive for surface modification (Plueddemann, 1991), as their bifunctional nature is expected to offer the possibility of covalently attaching a biomolecule, either directly or through a linker. 3-Aminopropyl(triethoxysilane) (APTES) is one of the most frequently used organosilane agents for the preparation of amine-terminated films (Asenath Smith & Chen, 2008; Howarter & Youngblood, 2006; Kim et al., 2009a; Lapin & Chabal, 2009; Pasternack et al., 2008).

Table 1 presents a list of references in which APTES was used to hopefully graft biomolecules on different substrates. The survey is exhaustive for stainless steeel substrates relevant for the field of biomaterials and illustrative for other substrates. Additional references are: El-Ghannam et al., 2004; Kim et al., 2010; Sasou et al., 2003; Sarath Babu et al., 2004; Quan et al., 2004 ; Subramanian et al., 1999 ; Jin et al., 2003 ; Cho & Ivanisevic, 2004 ; Katsikogianni & Missirlis, 2010 ; Sordel et al., 2007 ; Toworfe et al., 2006 ; Balasundaram et al., 2006 ; Doh & Irvine, 2006 ; Palestino et al., 2008 ; Son et al., 2011 ; Koh et al., 2006 ; Mosse et al., 2009 ; Weng et al., 2008 ; Charbonneau et al., 2011 ; Iucci et al., 2007 ; Chuang et al., 2006 ; Schuessele et al., 2009 ; Ma et al., 2007 ; Toworfe et al., 2009 ; Zile et al., 2011 ; Sargeant et al., 2008 ; Lapin & Chabal, 2009. Table 1 indicates the substrate and linker used, the main conditions of the APTES treatment and the evaluation of the surface treatment regarding biomolecule activity with the blank used for comparison. The table also presents the main data obtained by surface characterization. In some systems, no covalent grafting was aimed. In other systems, although it was aimed, there is no direct evidence for the formation of covalent bonds between the biomolecules and the substrate surface. On the other hand, the evaluation of the bio-efficacy was never based on comparisons involving a complete set of blanks: treatment with the biomolecule without silanization, without linker, without silanization and linker. In a study of surface modification with the aim to enhance mineralization, it has been demonstrated that APTES-coated glass retains a homopolymer with monoester phosphate groups, poly[(2-methacryloyloxy)ethyl phosphate], by proton transfer and electrostatic interaction, while the retention of a neutral homopolymer, poly[2-(acatoacetoxy)ethyl methacrylate], was attributed to covalent linkage by reductive amination between the keto groups of the polymer and the surface amine functions (Jasienak et al., 2009). The retention of the diblock copolymer seemed to occur via segments allowing covalent bonds to be formed. In Table 1, several systems show an improved behavior which may only be attributed to non covalent bonding between the biomolecule and the silanized substrate. In contradiction with frequent implicit considerations, the occurrence or improvement of bioactivity as a result of surface treatments does not demonstrate that the chemical schemes which motivated the treatments worked in reality. This question is crucial as many organic reactions that work well in solution are difficult to apply at solid surfaces (Kohli et al., 1998).

Stainless steels (SS) are extensively used in biomaterials researches and other applications involving contact with biologic compounds, owing to their adaptable mechanical properties, their manufacturability and their outstanding corrosion resistance. For instance, SS may be used in the manufacture of vascular stents, guide wires, or other orthopedic implants (Hanawa, 2002, Ratner, 2004). In these conditions, SS are subjected to the adsorption of biomolecules (proteins, polysaccharides, lipids) and biological materials (cellular debris). The surface modification of SS may thus be important to orient the host response as desired.
The present work is dedicated to the surface composition of 316L SS surfaces at different stages of the procedure used to graft a protein via the use of APTES and of a bifunctional agent expected to link the NH_2-terminated silane with NH_2 groups of the protein. Glucose oxidase was chosen as a model protein for reasons of convenience owing to previous works related to microbiologically influenced corrosion (Dupont et al., 1998, Landoulsi et al., 2009, Landoulsi et al., 2008b, Landoulsi et al., 2008c). A particular attention is given to (i) the real state of the interface (composition, depth distribution of constituents) at different stages and (ii) the mode of protein retention. Therefore, X-ray photoelectron spectroscopy is used in a way (angle resolved measurements, reasoned peak decomposition, validation by quantitative relationships between spectral data) to provide a speciation in terms of classes of compounds (silane, protein, contaminants), using guidelines established in previous works (Genet et al., 2008; Rouxhet & Genet, 2011). Water contact angle measurements are used to address the issue of the presence of contaminants and the perspectives of avoiding it.

Substrate	Linker	Biomolecule	Reference
a. Substrate preparation **b. APTES treatment** **c. Evaluation of efficiency regarding biomolecule activity. Substrate taken as blank** **d. Interface characterization**			
Stainless steel	EDC	Alginate	Yoshioka et al., 2003
a. Sonication in acetone, 5 min; heating 2 h at 500°C in air. b. In toluene, 1h; rinsing in toluene and ethanol; sonication in ethanol, 5 min; drying in air; curing 10 min at 105°C. c. Preventing adsorption of blood-clotting proteins. Blanks = native, silanized. d. XPS: elemental concentration, consistent evolution according to reaction steps; C 1s peak, demonstration of alginate retention, majority of carbon of C-(C,H) type at all stages.			
Stainless steel	GA	Lysozyme	Minier et al., 2005
a. Acid etching at 60 °C; rinsing in water; drying under N_2 gas flow. b. In ethanol/water, 3 min; curing 1 h at 100-150 °C in air; rinsing with water. c. Increase of the enzymatic activity in bacterial lysis. Blanks = native + enzyme, silanized + enzyme. d. IRRAS: Characteristic bands of APTES. XPS: elemental concentration, consistent evolution according to reaction steps; N/Si ratio vs photoelectron collection angle, consistent evolution.			
Stainless steel stent	none	Chitosan/heparin LbL film	Meng et al., 2009
a. Cleaning in ethanol/water (1/1, v/v); rinsing in water; drying under reduced pressure, 24 h at 30 °C. b. In ethanol, 4 h at 37 °C; rinsing in water, drying in air at 50 °C. c. Promoting re-endothelialization after stent implantation, improvement of			

haemocompatibility (in vivo and in vitro tests). Blank = native stainless steel stent, native+chitosan. d. QCM on model substrate slide: in situ monitoring of the LbL film growth on APTES-coated silicon substrate.			
Stainless steel screw	GA	Fibrinogen + bisphosphonate	North et al., 2004
a. Sonication in acetone; acid etching; treatment in H_2O_2/NH_4OH solution, 5 min at 80 °C. b. Vapor deposition, 10 min at 60 °C; curing 1 h at 150°C; sonication in xylene. c. Improvement of fixation of screws in rat tibia. Blank = test of bisphosphonate action. d. Ellipsometry on model substrate slide: consistent increase of the film thickness according to reaction steps.			
Titanium	SMP	RGDC peptide	Xiao et al., 1997
a. Acid etching; rinsing with different solvents; outgassing. b. In dry toluene, 120 °C, 3 h plus variants; sonication in various organic solvents and water. c. - d. Ellipsometry and radiolabeling: growth of silane surface layer upon repeating treatments. XPS peak shapes: semi-quantitatively consistent evolution according to reaction steps.			
Titanium	GA	Chitosan	Martin et al., 2007
a. Polishing; cleaning in different solvents followed by nitric acid passivation or piranha treatment. b. In toluene, 24 h; sonication in toluene, ethanol and water. c. - d. XPS: elemental concentration, consistent evolution according to reaction steps.			
Titanium	none	Heparin/fibronectin	Li et al., 2011
a. Polishing; sonication in different solvents, drying 2 h at 60 °C ; NaOH treatment, 2h at 80°C. b. In anhydrous ethanol, 10 h, sonication in ethanol; curing 6 h at 120 °C. c. Improvement of blood compatibility and promotion of endothelialization. Blanks = native, silanized. d. XPS : survey spectra consistent with treatments. AFM: small clumps after APTES step, and after APTES + protein step. Wet chemical analysis of proteins: consistent evolution according to reaction steps.			
Ti-6Al-4V	SMP	Cyclic peptides	Porté-Durrieu et al., 2004
a. Substrate oxidation; outgassing at 150 °C. b. In dry hexane under argon; rinsing with dry hexane; outgassing. c. Increase of osteoprogenitor cells attachment. Blanks = native, native + peptide. d. XPS: elemental concentration, consistent evolution according to reaction steps; N 1s peak, demonstration of peptide retention; C 1s peak, majority of carbon of C-(C,H) type at all stages.			
Co-Cr-Mo; Ti-6Al-4V	GA	Trypsin	Puleo, 1997
a. Cleaning in different solvent, acid passivation. b. In water 3 h or acetone 10 min; curing at 45 °C overnight. c. Decrease of the loss of enzymatic activity as a function of time for Co-Cr-Mo, no effect			

for Ti-6Al-4V. Blank = native + enzyme, silanized + enzyme. d. Wet chemical analysis of amino groups on silanized substrate only.			
Magnesium	Ascorbic acid	BSA	Killian et al., 2010
a. Surface polishing; rinsing in water and ethanol. b. In toluene, 24 h at 70 °C; rinsing in different solvents; sonication in ethanol. c. - d. XPS: elemental concentration, consistent evolution according to reaction steps. Tof-SIMS: demonstration of silanization and protein retention.			
Tantalum coating	DS3; DSS; DSC; CDI	Collagen	Müller et al., 2005
a. Acid etching; rinsing with different solvents; drying in vacuum. b. In boiling toluene under argon; rinsing in chloroform, methanol, and in water. c. Increase of cell adhesion and proliferation (stem cell culture and subcutaneous implantation). Blanks = native, silanized. d. Wet chemical analysis: amino groups, collagen, consistent with expectation. AFM: typical structure of fibrillar collagen.			
SiO_2, TiO_2, Si_3N_4	GA	Antigen	Kim et al., 2009b
a. Plasma treatment. b. In ethanol/water (95/5, v/v), rinsing with ethanol ; curing 15 min at 120 °C. c. Antigen/antibody test. Influence of plasma exposure time. d. Water contact angle and XPS on cleaned substrate, influence of plasma exposure time.			
Silicon dioxide	SMP	RGD peptide	Davis et al., 2002
a. Oxidation and hydroxylation; rinsing with different solvents. b. In dry toluene, 120 °C, 3 h; sonication in various organic solvents and water. c. Increase of fibroblast proliferation. Blanks = no RGD. d. XPS: elemental concentration, consistent evolution according to reaction steps. AFM: small clumps after APTES step ; larger clumps after APTES+SMP step.			
Silicon dioxide	GA	Glucose oxidase	Libertino et al., 2008
a. Oxidation in a solution of ammonia and hydrogen peroxide. b. Vapor deposition; curing 40 min at 80 °C under vacuum. c. Slight decrease of the enzyme activity when the surface is not oxidized (a). No blank. d. AFM: consistent evolution of surface roughness according to reaction steps. XPS: elemental concentration, consistent evolution according to reaction steps.			
Silicon dioxide	LC-SPDP	Tagged Kcoil peptides	Boucher et al., 2009
a. Piranha treatment, 10 min at 100°C; rinsing in water; drying in air; storing in vacuum. b. In anhydrous toluene, 3 h; curing 1.5 h at 120°C; sonication in freshly distilled toluene. c. Improvement of binding efficiency (amount, affinity) of Ecoil-tagged EGF. Blank = silanized + LC-SPDP with blocked termination. d. Ellipsometry and water contact angle: consistent evolution according to reaction steps.			
Glass	none	Proteins from ECM, RGD peptide	Siperko et al., 2006
a. Cleaning in different solvent. b. In anhydrous ethanol + acetic acid, followed by addition of ultrapure water, 5 min; curing 15 min at 120°C. c. Improvement of osteoblast adhesion and growth. Blank = silanized.			

d. AFM: increase of surface roughness, presence of nanostructures presumably due to proteins or peptide.			
Poly(dimethylsiloxane)	SSMCC	DNA	Vaidya & Norton, 2004
a. Surface plasma oxidation. b. Vapor deposition, 30 min, 100 °C. c. Hybridization of attached DNA. No blank. d. XPS: elemental composition and peak shapes, demonstration of silane deposition.			
Polystyrene	BS^3, GMBS	IgG	North et al., 2010
a. Plasma treatment. b. In ethanol+acetic acid; rinsing in methanol. c. - d. Fluorescence labeling: increase of amount of immobilized proteins by silanization + linker step.			
Cellulose	SMP	RGDC peptide	Bartouilh de Taillac et al., 2004
a. Drying, outgassing. b. In dry toluene under argon, 1.5 h; rinsing with dry toluene; outgassing. c. Increase of osteoprogenitor cells attachment and proliferation. Blank = native. d. XPS: qualitative consistency with expectations but probable Si contamination on final product.			

BSA = bovine serum albumin
BS^3 = bis(sulfosuccinimidyl) suberate
CDI = 1,1′-carbonyldimidazole
DSC = N,N′-disuccinimidyl-carbonate
DSS = N,N′-disuccinimidyl-suberate
DS3 = N,N′-disulphosuccinimidyl-suberate
EDC = 1-ethyl-3-(3-dimethylaminopropyl)carbodiimide.
ECM = extracellular matrix
EGF = epidermal growth factor
GA = glutaraldehyde
GMBS = 4-maleimidobutyric acid N-hydrosuccinimide ester
LbL = layer-by-layer
LC-SPDP = Succinimydil 6-[30-(2-pyridildithio)-propionamido]hexanoate
QCM = quartz crystal microbalance
RGDC = arginine - glycine - aspartic acid – cysteine
SMP = N-succinimidyl-3-maleimidopropionate
SSMCC = sulfosuccinimidyl-4-(N-maleimidomethyl)-cyclohexane-1-carboxylate
TNBS = 2,4,6-trinitrobenzenesulfonic acid

Table 1. Illustration of the use of APTES for retaining biomolecules on surfaces. The meaning of a, b, c, and d is given in the upper box.

2. Materials and methods

2.1 Materials

Disks of 316L SS (0.74 cm^2, from Outokumpu Stainless AB, ARC) were used. The bulk chemical composition of 316L SS was given previously (Landoulsi et al., 2008a). All chemicals (NaCl, Na_2SO_4, $NaNO_3$ $NaHCO_3$, $NaHPO_4$, Na_2PO_4) were provided by Prolabo (VWR, France) and ensured 99% minimum purity. 3-aminopropyl(triethoxysilane) (APTES, 99%), glucose oxidase (Gox, EC 1.1.3.4, 47200 $U.g^{-1}$) from *Aspergillus Niger* and *D*-glucose

were purchased from Sigma-Aldrich (France). Bis(sulfosuccinimidyl) suberate (BS) was purchased from Pierce (Rockford, IL, USA).

2.2 Stainless steel surface preparation

The samples (both faces and perimeter) were polished with 1 μm diamond suspension (Struers, Denmark), rinsed in binary mixture of milliQ water/ethanol (1/1, v/v) in a sonication bath (70W, 40 kHz, Branson, USA) and dried under nitrogen gas flow.The samples were then immediately immersed for 48 h in synthetic aqueous medium (NaCl 0.46 mmol.L^{-1}, Na_2SO_4 0.26 mmol.L^{-1}, $NaNO_3$ 0.2 mmol.L^{-1}, $NaHCO_3$ 3.15 mmol.L^{-1}, pH about 8), abundantly rinsed with milliQ water (Millipore, Molsheim, France) and dried under nitrogen gas flow. These samples are considered as native SS and designated as "nat".

2.3 Surface treatment procedure

The silanization of nat samples was performed in the gas phase with APTES. To this end, nat samples were placed, together with a small vial containing 100 μL APTES, in a 7 dm^3 closed recipient under vacuum for 30 min at room temperature. The samples were cured for 1 h at 100°C under vacuum, rinsed and incubated for 6 h in milliQ water to eliminate the excess of non attached silanes. These are called "sil".

Both nat and sil samples were subjected to treatments with the coupling agent (BS) and/or the enzyme (Gox) as detailed below:

i. "+BS" and "sil+BS" obtained after BS treatment (10 mM in milliQ water) for 30 min on nat and sil samples, respectively,
ii. "+Gox" and "sil+Gox" obtained after Gox treatment (0.1 mg.mL^{-1} in phosphate buffer pH~6.8) for 2 h, on nat and sil samples, respectively,
iii. "+BS+Gox" and "sil+BS+Gox" obtained after both BS and Gox treatment (according to the procedure described above) on nat and sil samples, respectively.

After BS or Gox treatment, the samples were rinsed three times with milliQ water and dried under nitrogen gas flow.

In order to clarify the issue of surface contamination, nat samples were further cleaned by UV-ozone treatment (UVO Cleaner, Jelight Co, Irvine, Ca, USA) during 20 minutes. They were then placed in a Petri dish, left in the laboratory environment, and submitted to water contact angle measurements as a function of time.

2.4 X-ray photoelectron spectroscopy

XPS analyses were performed using a Kratos Axis Ultra spectrometer (Kratos Analytical, UK), equipped with a monochromatized aluminum X-ray source (powered at 10 mA and 15 kV) and an eight channeltrons detector. No charge stabilization device was used on these conductive samples. Analyses were performed in the hybrid lens mode with the slot aperture; the resulting analyzed area was 700 μm × 300 μm. A pass energy of 40 eV was used for narrow scans. In these conditions, the full width at half maximum (FWHM) of the Ag $3d_{5/2}$ peak of clean silver reference sample was about 0.9 eV. The samples were fixed on the support using a double-sided adhesive conducting tape. The pressure in the analysis chamber was around 10^{-6} Pa. The photoelectron collection angle θ between the normal to the sample surface and the electrostatic lens axis was 0° or 60°. The following sequence of spectra was recorded: survey spectrum, C 1s, O 1s, N 1s, P 2p, Cr 2p, Fe 2p, Ni 2p, Mo 3d, Na 1s, S 2p, Si 2p and C 1s again to check for charge stability as a function of time, and absence of sample degradation. The binding energy scale was set by fixing the C 1s

component due to carbon only bound to carbon and hydrogen at 284.8 eV. The data treatment was performed with the Casa XPS software (Casa Software Ltd., UK). The peaks were decomposed using a linear baseline, and a component shape defined by the product of a Gauss and Lorentz function, in the 70:30 ratio, respectively. Molar concentration ratios were calculated using peak areas normalized according to the acquisition parameters and the relative sensitivity factors and transmission functions provided by the manufacturer.

2.5 Atomic force microscopy (AFM)

The surface topography was examined using a commercial AFM (NanoScope III MultiMode AFM, Veeco Metrology LLC, Santa Barbara, CA) equipped with a 125 μm × 125 μm × 5 μm scanner (J-scanner). A quartz fluid cell was used without the O-ring. Topographic images were recorded in contact mode using oxide-sharpened microfabricated Si_3N_4 cantilevers (Microlevers, Veeco Metrology LLC, Santa Barbara, CA) with a spring constant of 0.01 $N.m^{-1}$ (manufacturer specified), with a minimal applied force (<500 pN) and at a scan rate of 5-6 Hz. The curvature radius of silicon nitride tips was about 20 nm. Images were obtained at room temperature (21-24°C) in milliQ water. All images shown in this paper were flattened data using a third order polynomial. The surface roughness (R_{rms}) was computed over an area of 1 μm × 1 μm using the Veeco software.

2.6 Water contact angle measurements

Water contact angles were measured at room temperature using the sessile drop method and image analysis of the drop profile. The instrument, using a CCD camera and an image analysis processor, was purchased from Electronisch Ontwerpbureau De Boer (The Netherlands). The water (milliQ) droplet volume was 0.3 μL, and the contact angle was measured 5 s after the drop was deposited on the sample. For each sample, the reported value is the average of the results obtained on 5 droplets.

3. Results

AFM images obtained in water on SS samples after different treatments are presented in Figure 1. The nat sample showed the presence of nanoparticles with different sizes (nat, Figure 1, R_{rms} = 3.2 nm), in agreement with previous results. The formation of nanoparticles, presumably made of ferric hydroxide, resulted from oxidation occurring during the 48 h of immersion subsequent to polishing (Landoulsi et al., 2008a). The surface of silanized SS exhibited particles with a bigger size (sil, Figure 1) and the roughness decreased slightly (sil, Figure 1, R_{rms} = 2.4 nm). The treatment with Gox, with or without previous treatment with BS, led to the formation of particles with a more uniform size and a higher density, in comparison with nat sample, and no appreciable change of surface roughness (R_{rms} = 1.7 nm for sil+Gox and 2.5 nm for sil+BS+Gox, Figure 1).

XPS is a suitable method to obtain information regarding the different constituents at the surface (substrate, silane, other organic compounds). The elemental composition of the samples is given in Table 2. Representative C 1s and O 1s peaks recorded on SS surface prior to and after silanization, and after further treatments are given in Figure 2. After BS and/or Gox treatment of silanized SS, a relative increase of the component around 531.2 eV in the O 1s peak was observed (Figure 2). In the C 1s peak, an increase of the components at 286.3 and 288.7 eV was also clear, while the main component remained at 284.8 eV. The same

tendency regarding the C 1s and O 1s peaks was also observed after BS and/or Gox treatment of nat sample, but was less pronounced (data not shown). It may be attempted to

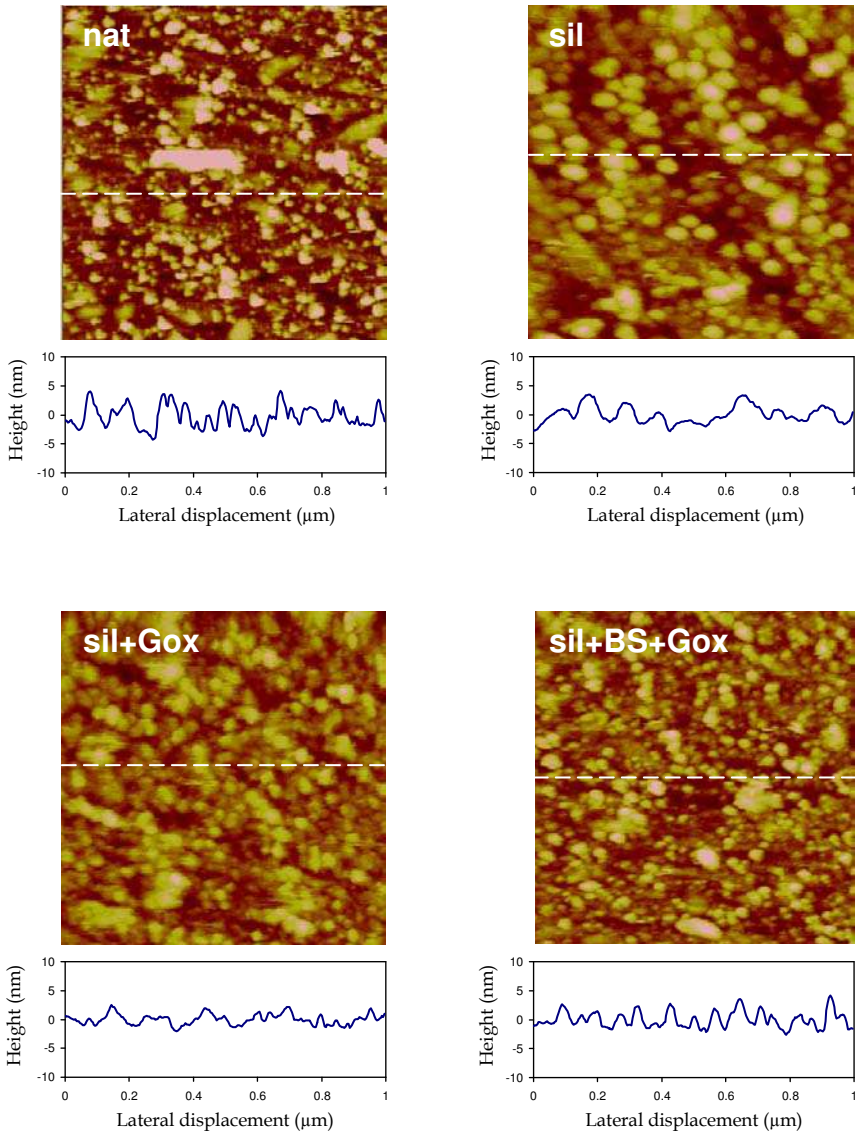

Fig. 1. AFM height images (1×1 µm², contact mode, in water; z scale 10 nm) of native (nat), silanized stainless steel (sil), the same after adsorption of glucose oxidase (sil+Gox) and after treatment with glucose oxidase subsequent to treatment with the coupling agent (sil+BS+Gox). Cross sections were taken at the place indicated by the dashed lines.

extract chemical information by careful decomposition of the peaks. This requires to impose reasonable constraints (number of components, full width at half maximum FWHM) in order to insure reliable comparisons, and to check the chemical relevance of the results by examining correlations between spectral data of different natures (Genet et al., 2008; Rouxhet & Genet, 2011). In previous studies (Landoulsi et al., 2008a; Landoulsi et al., 2008b), we have demonstrated the usefulness of this approach, even when the evolution of the C 1s and O 1s peak shape is weak, in order to obtain information on the amount and the nature of organic and inorganic constituents on SS surfaces.

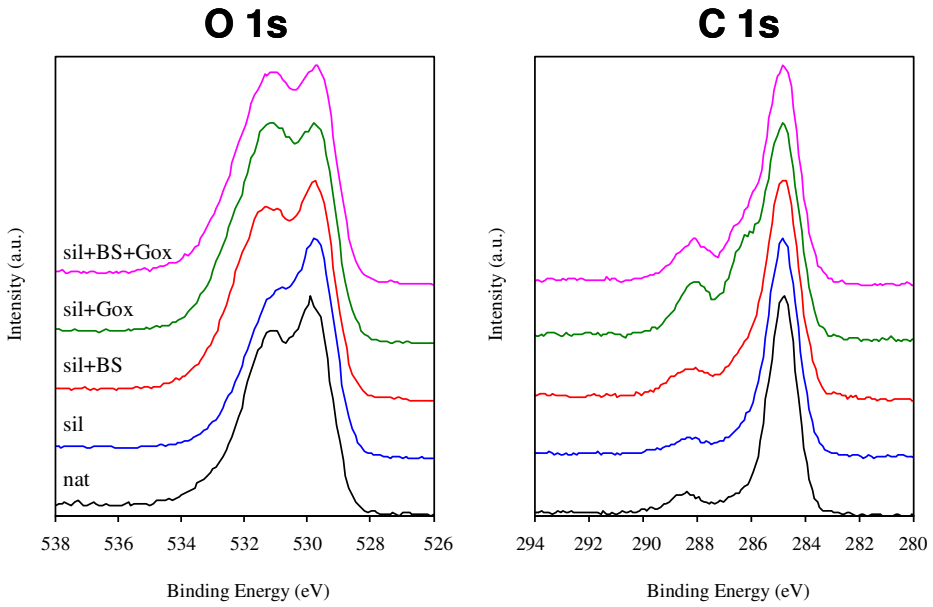

Fig. 2. O 1s and C 1s peaks of native (nat), of silanized stainless steel (sil), of the same after treatment with the coupling agent (sil+BS), after adsorption of glucose oxidase (sil+Gox) and after treatment with glucose oxidase subsequent to treatment with the coupling agent (sil+BS+Gox).

Figure 3 presents typical O 1s, N 1s and C 1s XPS peaks recorded on native SS (nat), silanized (sil) and the same after Gox treatment (sil+Gox). For the decomposition of these peaks, reasonable constraints were applied, based on our experience with the XPS analysis of biosurfaces (Genet et al., 2008, Rouxhet & Genet, 2011). The C ls peak was decomposed in four components, the FWHM of which were imposed to be equal: (i) a component at 284.8 eV due to carbon only bound to carbon and/or hydrogen [C–(C,H)]; (ii) a component at about 286.3 eV due to carbon making a single bond with oxygen and/or nitrogen [C–(O,N)] in alcohol, amine, or amide; (iii) a component at 287.8 eV due to carbon making one double bond or two single bonds with oxygen (C=O, O–C–O) and (iv) a component at 288.7 eV attributed to carboxyl or ester functions [(C=O)–O–R].

The O 1s peak was decomposed in three components (Landoulsi et al., 2008a). The first one, at 529.7 eV, is due to inorganic oxygen in metal oxides (M–O) (NIST Database). The FWHM of the two other components were arbitrarily imposed to be equal. The component at about 531.2 eV may be due to oxygen making a double bond with carbon (C=O including amide and carboxyl group) and to oxygen of carboxylate. Contributions of metal hydroxides (M–O–H) as well as oxygen bound to silicon [Si–O] in silane are overlapping with this component (NIST Database; Genet et al., 2008). The last component, at 533.1 eV, is attributed to oxygen making single bonds with carbon (C–O–H of alcohol and carboxyl, C–O–C of ether and ester).

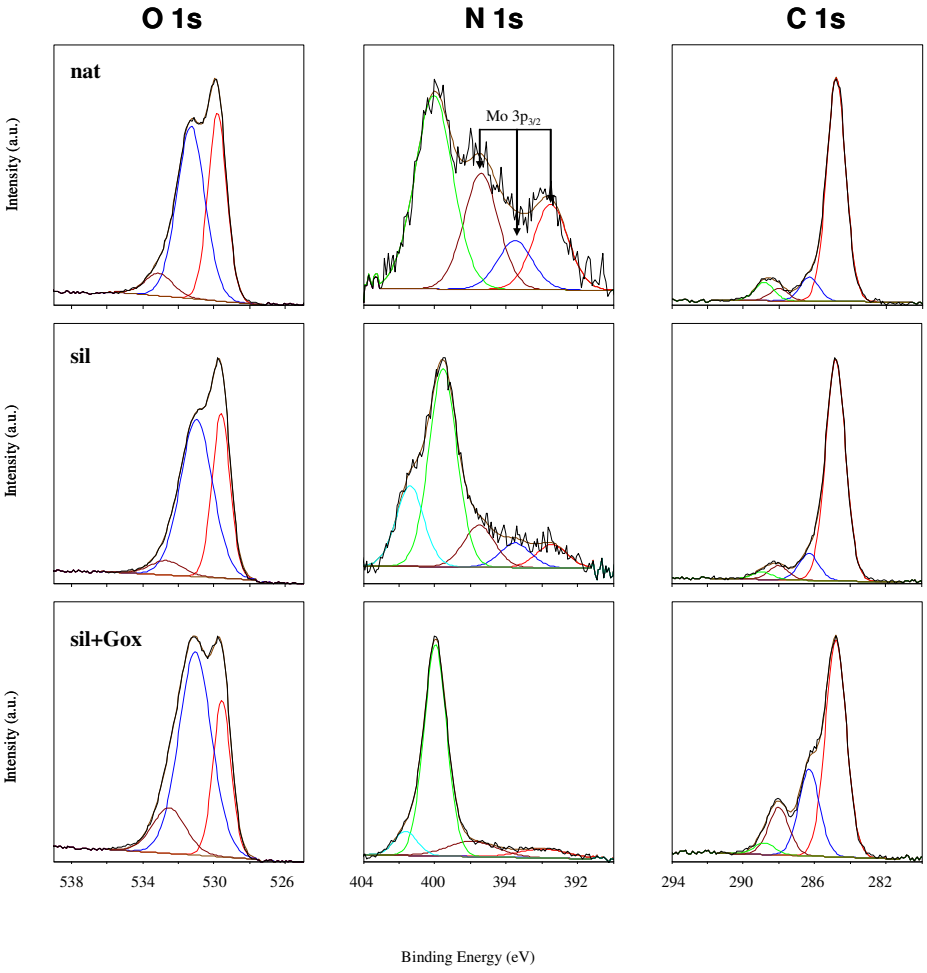

Fig. 3. Decomposition of O 1s, N 1s and C 1s peaks recorded on: native stainless steel (nat), silanized stainless steel (sil) and the same after adsorption of glucose oxidase (sil+Gox). The N 1s peak is overlapped with a Mo $3p_{3/2}$ contribution.

The N 1s peak showed a main component at 400.0 eV attributed to amide or amine (N–C). An additional component appeared clearly near 401.6 eV in silanized SS samples (sil and sil+Gox, Figure 3), indicating the presence of protonated amines. The contributions at lower binding energies in the N 1s spectral window are due to Mo $3p_{3/2}$ components (Olefjord & Wegrelius, 1996); the reliability of their quantification was checked by comparison with the Mo concentration deduced from the Mo $3p_{3/2}$ and Mo 3d peaks (Landoulsi et al., 2008a). The N 1s contribution of sil shows a shape which is in agreement with spectra reported in the literature for APTES-modified surfaces (Suzuki et al., 2006; Xiao et al., 1997). It was not found justified to decompose it in three components attributed to amine, amide and protonated amine, respectively, as done in (Suzuki et al., 2006). The surface concentrations (mole fraction) associated with the components of C 1s, O 1s and N 1s peaks are given in Table 2.

	Ni^{ox}	Ni^{met}	Ni_{tot}	Fe^{ox}	Fe^{met}	Fe_{tot}	Cr^{ox}	Cr^{met}	Cr_{tot}	Mo^{ox}	Mo^{met}	Mo_{tot}	Si^0
nat	1.23	0.73	**1.95**	7.59	1.57	**9.16**	4.69	0.33	**5.02**	0.34	0.12	**0.46**	**0.38**
+BS	0.81	0.54	**1.35**	8.32	1.89	**10.21**	5.96	0.40	**6.36**	0.46	0.12	**0.57**	**0.29**
+Gox	0.59	0.51	**1.10**	8.63	1.70	**10.33**	5.53	0.33	**5.86**	0.37	0.12	**0.49**	**-**
+BS+Gox	0.66	0.39	**1.05**	8.90	1.43	**10.33**	4.56	0.30	**4.87**	0.32	0.12	**0.44**	**0.36**
sil	0.47	0.33	**0.80**	7.89	1.22	**9.10**	4.59	0.27	**4.86**	0.31	0.10	**0.40**	**0.37**
sil+BS	0.47	0.43	**0.91**	6.91	1.45	**8.36**	5.24	0.33	**5.57**	0.35	0.11	**0.45**	**0.32**
sil+Gox	0.60	0.38	**0.98**	6.14	1.29	**7.42**	4.95	0.29	**5.23**	0.32	0.12	**0.44**	**0.26**
sil+BS+Gox	0.54	0.32	**0.86**	6.22	1.16	**7.39**	4.58	0.24	**4.82**	0.34	0.09	**0.42**	**0.30**

	$C_{288.7}$	$C_{287.8}$	$C_{286.3}$	$C_{284.8}$	C_{tot}	$O_{533.1}$	$O_{531.2}$	$O_{529.7}$	O_{tot}	O_{org}	$N_{401.6}$	N_{400}	N_{tot}	Si_{org}	$\sum org$
nat	2.45	2.29	3.92	39.62	**48.28**	2.36	19.02	12.60	**33.98**	**7.92**	0.00	0.73	**0.73**	**0.44**	**57.37**
+BS	2.89	2.08	3.88	34.87	**43.71**	2.48	18.96	13.86	**35.30**	**7.64**	0.00	1.21	**1.21**	**0.43**	**52.99**
+Gox	2.03	2.16	4.78	35.56	**44.53**	2.97	20.96	11.27	**35.20**	**7.50**	0.13	1.34	**1.48**	**-**	**53.50**
+BS+Gox	2.55	2.60	5.89	30.02	**41.06**	3.96	22.01	12.57	**38.54**	**9.46**	0.23	1.35	**1.58**	**0.89**	**52.99**
sil	1.15	2.37	4.57	36.13	**44.23**	1.95	21.22	12.28	**35.45**	**5.93**	0.63	1.54	**2.17**	**2.29**	**54.61**
sil+BS	2.03	3.30	6.48	32.72	**44.53**	1.07	23.16	9.71	**33.94**	**8.49**	0.66	2.65	**3.31**	**2.13**	**58.47**
sil+Gox	1.18	5.97	10.39	25.08	**42.62**	4.74	21.09	8.86	**34.70**	**11.78**	0.59	5.16	**5.75**	**1.74**	**61.90**
sil+BS+Gox	1.46	4.89	8.31	30.39	**45.05**	2.87	22.24	8.52	**33.63**	**9.86**	0.50	4.30	**4.80**	**2.01**	**61.72**

Table 2. Surface concentration (mole fraction (%) computed over the sum of all elements except hydrogen) of elements determined by XPS (θ = 0°) on stainless steel samples.

The Si 2p peak was decomposed in two components, at 99.3 and 101.8 eV, attributed to non oxidized silicon in SS (Si^0) and to silicon of silane (Si_{org}), respectively. It was not decomposed in Si $2p_{3/2}$ and Si $2p_{1/2}$ contributions because these are very close in energy. The decomposition procedure for Fe $2p_{3/2}$, Cr 2p, Ni $2p_{3/2}$, and Mo 3d peaks was described before (Landoulsi et al., 2008a). The Fe concentration may be underestimated due to the procedure used to treat the complex baseline of the Fe 2p peak. The distinction between contributions of oxidized (M^{ox}) and nonoxidized (M^{met}) metal elements was easily made. The concentrations obtained are also given in Table 2.

The concentration of oxygen present in organic compounds O_{org} may not directly be deduced from the O 1s peak owing to the overlap with inorganic hydroxide. However, for biological systems the sum of O and N concentrations may be evaluated by the

concentration of carbon in oxidized form, C_{ox}, in consistency with alcohol, primary amine, primary amide and ester functions. Accordingly,

$$O_{org} = C_{ox} - N = C_{286.3} + C_{287.8} + C_{288.7} - N_{tot} \quad (1)$$

where the name of an element in italic designates its concentration and the number in subscript designates the binding energy of the peak component. Errors would occur in case of a high concentration of polysaccharides ($C_{ox}/O = 6/5$) or carboxyl ($C_{ox}/O = 1/2$) (Genet et al., 2008 ; Landoulsi et al., 2008a).
The sum of the concentrations of the elements present in organic compounds is then given by:

$$\sum org = C_{tot} + O_{org} + N_{tot} + Si_{org} = C_{tot} + C_{ox} + Si_{org} \quad (2)$$

For sake of uniformity, all spectral data involved in correlations below are ratioed to $\sum org$ (Table 2).
The concentration of the main elements or functions due to organic compounds, obtained at photoelectron collection angle $\theta = 0°$, is plotted in Figure 4 as a function of the same quantity obtained at $\theta = 60°$. A 1:1 relationship is obtained for all elements or functions and all samples, indicating no significant effect of the photoelectron collection angle θ on the relative contribution of the constituents of the organic adlayer.

4. Discussion

4.1 Passive film composition

Table 2 shows that the apparent concentrations of metal elements varied only slightly according to the surface treatment. The main change concerned the decrease of the Fe^{ox} concentration for sil+BS, sil+Gox and sil+BS+Gox samples. However, no change in the shape of the Fe $2p_{3/2}$ peak was observed (data not shown). For these samples, a significant decrease of the molar concentration of $O_{529.7}$ was also noticed (Table 2). It appears that the oxide layer of SS passive film, after incubation in the aqueous medium for 48 h (nat sample), was mainly constituted with a mixture of Fe and Cr oxides/hydroxides and small amounts of partially oxidized Ni and Mo. This is in agreement with a previous study (Landoulsi et al., 2008a), however in the latter, the stoichiometry of the passive film was not computed.
The O 1s component at 529.7 eV is due to metal oxides. By considering that Mo^{ox} is in the form of MoO_3 (Landoulsi et al., 2008a), the difference between the $O_{529.7}$ concentration and three times the Mo^{ox} concentration should be due to Fe and Cr oxides. Figure 5 presents the relation between this difference and the sum of Fe^{ox} and Cr^{ox} concentrations. All data show reasonable linear regressions. The shift of the dots along the line when the photoelectron collection angle changes from 0° to 60° is due to the presence of the organic constituents on top of stainless steel. The average ratio between the y and x scales is 0.80 and 0.96 at $\theta = 0$ and 60°, respectively; the slope of the regression lines is 1.03 (s.d. 0.23) and 1.42 (s.d. 0.12), respectively. Thus, the ratio oxide/metal ions in chromium and iron oxyhydroxides is of the order of 1 to 1.5.
The evaluation of the quantity of hydroxide associated to Fe and Cr is complex due to the multiple chemical functions overlapping in the $O_{531.2}$ component. Ni^{ox} is in the form of $Ni(OH)_2$ (component at ~855.6 eV (Briggs & Seah, 1990, Zhou et al., 2006), spectra not shown). The amount of oxygen associated to silane depends on the products of APTES

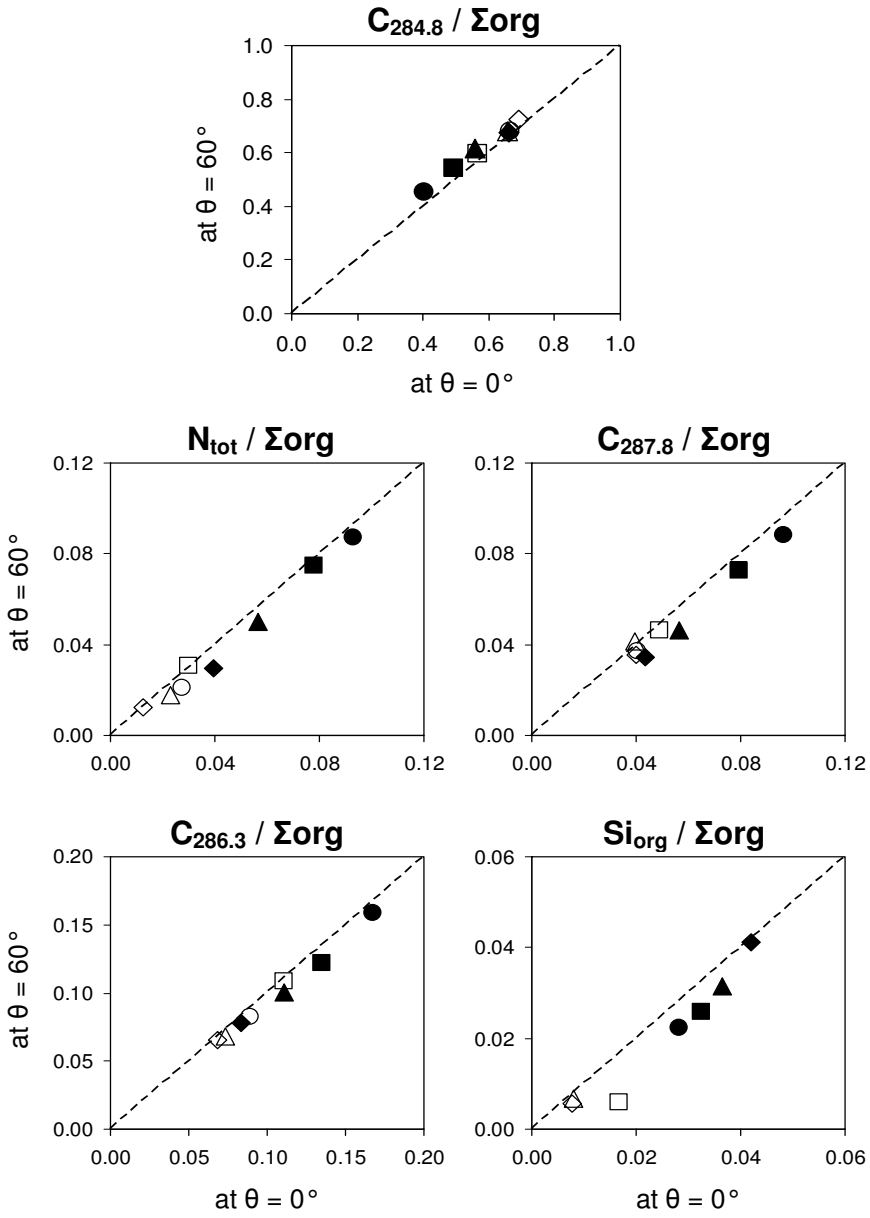

Fig. 4. Plots of molar concentrations ratioed to the sum of organic elements (Σorg) measured by XPS at θ = 60° *vs* θ = 0° on native (open symbols) or silanized stainless steel (closed symbols), as such (◆,◇) or further treated with coupling agent BS (▲,△), glucose oxidase (●,○) or coupling agent followed by glucose oxidase (■,□). The dashed lines represent a *y*/*x* ratio of 1:1.

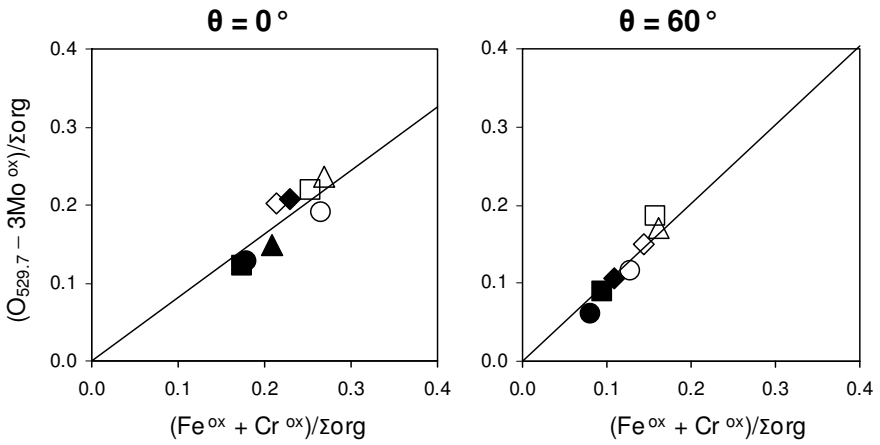

Fig. 5. Relations between molar concentrations ratioed to the sum of organic elements (Σorg) measured by XPS at θ = 0° (data from Table 2) and θ = 60° on native (open symbols) or silanized stainless steel (closed symbols), as such (◆,◇) or further treated with coupling agent BS (▲,△), glucose oxidase (●,○) or coupling agent followed by glucose oxidase (■,□).

reaction. The different possibilities, corresponding to the relative importance of grafting with respect to polymerization, are shown in Figure 6 and characterized by a, defined as the sum, over oxygen atoms which are not bound to a metal element, of the inverse of the number of bonds oxygen forms with silicon. Accordingly the concentration of inorganic hydroxide in the passive film may be given as follows:

$$OH_{inorg} = O_{tot} - O_{org} - O_{529.7} - a \times Si_{org} \quad (3)$$

where a can take the values of 0, 0.5, 1, 1.5 or 2 (Figure 6).

Figure 7 shows the plot of the concentration of hydroxide which should be associated with Fe and Cr, considering different values of a. Taking silicon into account ($a \neq 0$) brings the silanized substrates better in line with the non-silanized substrates and the correlation improves as a increases, indicating that silane is polymerized and not just grafted. Depending on the value of a, the $y : x$ ratio varies from 1.1 ($a = 0$) to 0.8 ($a = 2$).

These observations indicate that the stoichiometry of the Cr and Fe oxyhydroxide at the surface is close to (Fe,Cr)OOH. Many studies have reported a stratification in the passive film and the presence of Fe and Cr oxyhydroxides in the outermost layer (Le Bozec et al., 2001). In our case, no significant effect of the photoelectron collection angle appears in the $OH_{inorg}/O_{529.7}$ ratio (Figure 8), whatever the value selected for a to evaluate OH_{inorg}. However it must be kept in mind that the surface roughness revealed by Figure 1, which is of the order of the inelastic mean free path of photoelectrons in oxides, may mask the effect of a stratification.

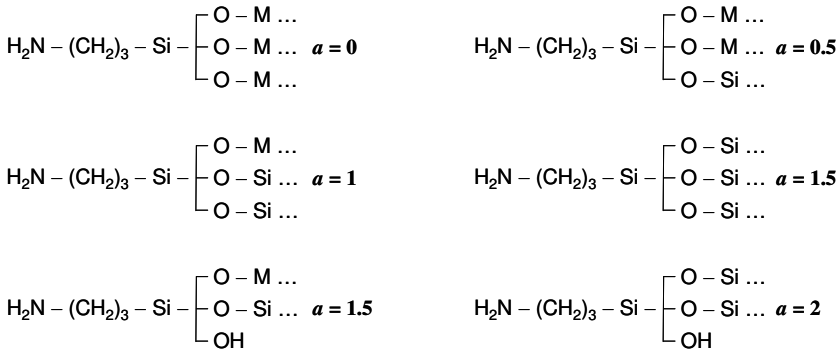

Fig. 6. Possible products of APTES reaction. "M" designates metal elements of stainless steel.

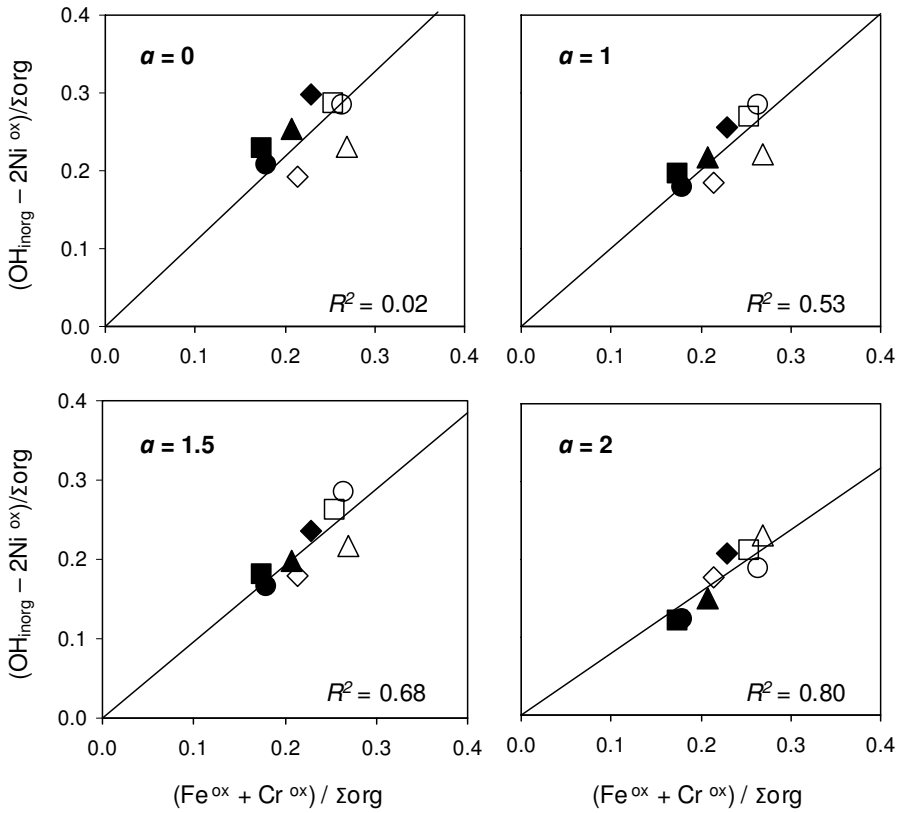

Fig. 7. Relations between molar concentrations ratioed to the sum of organic elements (Σorg) measured by XPS at θ = 0° (data from Table 2) on native (open symbols) or silanized stainless steel (closed symbols), as such (◆,◇) or further treated with coupling agent BS (▲,△), glucose oxidase (●,○) or coupling agent followed by glucose oxidase (■,□).

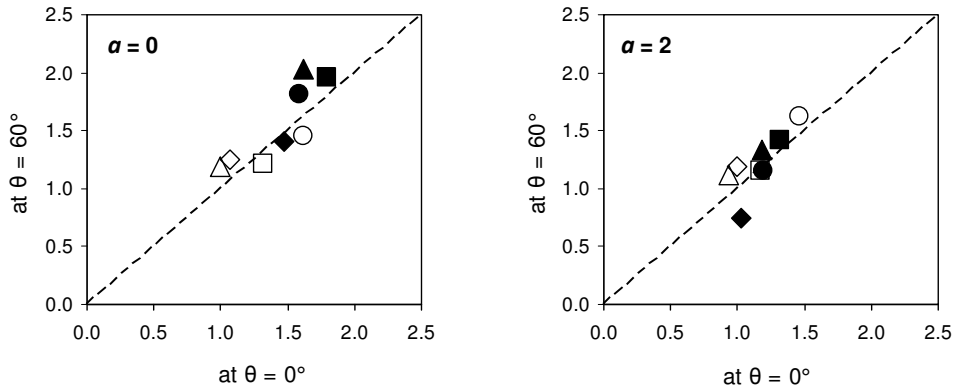

Fig. 8. Plots of OH_{inorg} / $O_{529.7}$ ratio measured by XPS at θ = 60° *vs* θ = 0° on native (open symbols) or silanized stainless steel (closed symbols), as such (◆,◇) or further treated with coupling agent BS (▲,△), glucose oxidase (●,○) or coupling agent followed by glucose oxidase (■,□). The dashed lines represent a *y/x* ratio of 1:1.

4.2 Chemical speciation of the organic adlayer

Table 2 reveals an increase of N_{tot} concentration as a result of surface treatments, and an increase of Si_{org} concentration for samples prepared with APTES treatment. However, the concentration of carbon is high and remains almost unchanged, suggesting that organic contaminants, mainly hydrocarbon-like compounds, are always dominating in the organic adlayer. If nitrogen was exclusively due to amide functions (N-C=O) as in the peptide link of proteins, and if the C 1s component at 287.8 eV was exclusivley due to amide, a 1:1 correlation would be found between the concentrations of $C_{287.8}$ and N_{tot}. This is indeed observed (Figure 9a) for the set of samples involving the silanized substrate. As nitrogen is partly in the form of silane, relevant alternatives for the abscissa scale may be the concentration of N_{400} or the difference between the concentrations of N_{tot} and Si_{org}. If polysaccharides were present with protein, the $C_{287.8}$ concentration should be corrected by subtracting the contribution of acetal and thus replaced by $[C_{287.8} - (C_{286.3} - N_{400})/5]$ (Ahimou et al., 2007, Landoulsi et al., 2008a) or $[C_{287.8} - (C_{286.3} - N_{tot} + Si_{org})/5]$. A comparison between different plots in Figure 9 shows that the dots representative of samples prepared with non-silanized substrate remain clustered. The shift of the cluster along the ordinate scale according to the plot indicates that $C_{287.8}$ concentration is higher than what can be attributed to amide. On the other hand, the samples prepared with silanized substrate preserve a unit slope whatever the plot, with much higher values of the coordinates for samples exposed to the enzyme, with or without the linker. This reveals an excellent agreement between the increases of concentrations of nitrogen and of carbon attributed to peptidic links (N−C=O), which result from the Gox treatment. It also validates the C 1s peak decomposition and component attribution.

The meaning of the surface composition appears more clearly if it is summarized in terms of concentration of model molecular compounds. This approach was already used for microbial surfaces (Dufrêne & Rouxhet, 1996; Tesson et al., 2009), for food products (Rouxhet et al., 2008) and for stainless steel aged in different conditions (Landoulsi et al.,

2008b), considering proteins (Pr), polysaccharides (PS), and hydrocarbon-like compounds (HC) which represent mainly lipids in biological systems. The novelty here is to take silane (Sl) into account in addition to the three classes of biochemical compounds; the chemical composition and density considered for these model compounds are listed in Table 3. Accordingly, the proportion of carbon atoms due to each model compound X (C_X/C_{tot}) can be computed by solving the following system of equations:

$$(N_{tot} - Si_{org})/C_{tot} = 0.273 \times (C_{Pr}/C_{tot}) \quad (4)$$

$$O_{org}/C_{tot} = 0.312 \times (C_{Pr}/C_{tot}) + 0.833 \times (C_{PS}/C_{tot}) \quad (5)$$

$$Si_{org}/C_{tot} = 0.333 \times (C_{Sl}/C_{tot}) \quad (6)$$

$$1 = (C_{Pr}/C_{tot}) + (C_{PS}/C_{tot}) + (C_{Sl}/C_{tot}) + (C_{HC}/C_{tot}) \quad (7)$$

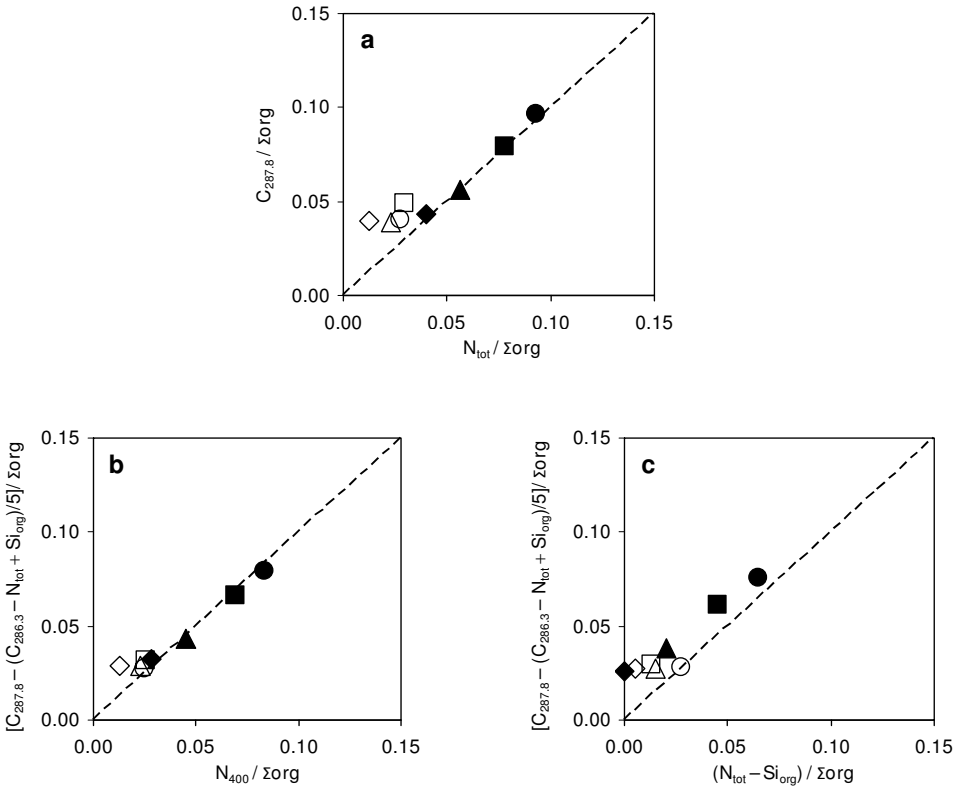

Fig. 9. Relations between molar concentrations ratioed to the sum of organic elements (Σorg) measured by XPS at θ = 0° (data from Table 2) on native (open symbols) or silanized stainless steel (closed symbols), as such (◆,◇) or further treated with coupling agent BS (▲,△), glucose oxidase (●,○) or coupling agent followed by glucose oxidase (■,□).The dashed lines represent a *y/x* ratio of 1:1.

The experimental concentration ratios (C_X/C_{tot}) can be converted into weight percentages of model compounds (Genet et al., 2008, Rouxhet & Genet, 2011), using the carbon concentration specific to each compound (Table 3).

	O/C	N/C	Carbon concent. (mmol.g^{-1})	Density (g.cm^{-3})
Proteins	0.312 *	0.273 *	43.5	1.4
Silane	0.5	0.333	27.3	0.9
Polysaccharides	0.833	-	37.0	1.5
Hydrocarbons	-	-	71.4	0.9

* Data computed from the amino acid sequence of glucose oxidase on the basis of ProtParam tool available on the ExPASy molecular biology server (http://us.expasy.org).

Table 3. Chemical composition of organic compounds (molar concentration ratio of elements and concentration of carbon) and their densities.

Results, presented in Table 4, show the often dominating presence of hydrocarbon-like compounds and polysaccharides, for all samples. Both compounds are due to adventitious contamination which may originate from adsorption from air, as always observed for high surface energy solids (Caillou et al., 2008; Mantel et al., 1995), but also from aqueous media (Landoulsi et al., 2008a). They may be taken as a global way to reflect the amount of compounds which contain hydrocarbon chains and oxygen, such as esters, but excluding proteins and silane. The concentration of silane deduced for non-silanized samples is non negligible but highly variable, and may also be attributed to contamination. A drastic increase of silane concentration is observed for all silanized samples (Table 4).

	(wt. %)				Thickness (nm)	
	Pr	Sl	PS	HC	at θ = 0°	at θ = 60°
nat	2.9	5.8	29.5	61.7	3.6	2.2
+BS	(8.5)	6.1	28.3	57.1	3.2	2.1
+Gox	16.3	0.0	24.7	59.0	3.2	2.3
+BS+Gox	(7.3)	12.3	35.5	44.9	3.3	2.2
sil	0.0	29.0	22.2	48.8	3.8	2.7
sil+BS	(10.8)	25.5	25.2	38.5	3.9	2.8
sil+Gox	35.2	20.0	24.3	20.5	3.9	2.9
sil+BS+Gox	24.4	22.9	22.5	30.2	4.1	2.8

* The data between brackets are protein equivalent of BS products and have no physical meaning.

Table 4. Chemical composition (weight %) of the organic adlayer present on stainless steel samples, as deduced from XPS data and expressed in terms of classes of molecular compounds*. Thickness of the organic adlayer deduced from measurements at photoelectron collection angle θ = 0° and 60°.

The Gox treatment leads to a marked increase of the protein concentration on nat sample and a much stronger increase on sil sample. This may be attributed to physical adsorption

and to the fact that protonated amine of silane favors adsorption by electrostatic attraction (Jasienak et al., 2009). The pH of the Gox solution (6.8) is indeed higher than the isoelectric point of glucose oxidase (4.9).

In the above computation, the concentration of the BS coupling agent could not be evaluated. The reaction of BS with NH_2 transforms an amine function into amide. If only one end of BS reacts with silane, the N_{400} concentration should be doubled, which is consistent with the increase found in Table 2. However, converting it into protein-equivalent gives a number with no physical meaning. When the second end of the coupling agent reacts with the protein, no additional nitrogen is incorporated, the evaluation of the protein concentration is correct but the suberate $(CH_2)_6$ chain is counted in the HC concentration. This has no important impact owing to the high concentration of hydrocarbon-like compounds. Despite the limitations regarding the accuracy of the data in Table 4, it is clear that prior silanization increases markedly the concentration of glucose oxidase (sil+Gox and sil+BS+Gox compared to nat+Gox); however the treatment with the coupling agent does not increase the amount of immobilized enzyme (sil+BS+Gox compared to sil+Gox).

4.3 State of stainless steel surface

It appears in Table 4 that the SS surface prior to and after silanization or enzyme immobilization is bearing a high amount of organic contaminants. It may be argued that this is due to improper cleaning protocols, inappropriate sample manipulation or contamination in the XPS spectrometer. Actually, a clean stainless steel surface is getting quickly contaminated in contact with the surrounding atmosphere, as revealed by water contact angles, which can be measured quickly in the same environment. A nat sample showed a water contact angle of 44° which increased to about 60° within a delay of a few hours (Figure 10). When a nat sample was further treated with UV-ozone to oxidize organic compounds, the water contact angle was lowered down to 12°. However it increased rapidly in contact with the surrounding atmosphere (Figure 10) to reach values above 40° in a few hours. Similar results were obtained with 304L stainless steel. Wet cleaning essentially standardizes the surface contamination; further cleaning leaves a material with a high surface energy, which adsorbs quickly significant amounts of contaminants (Caillou et al., 2008).

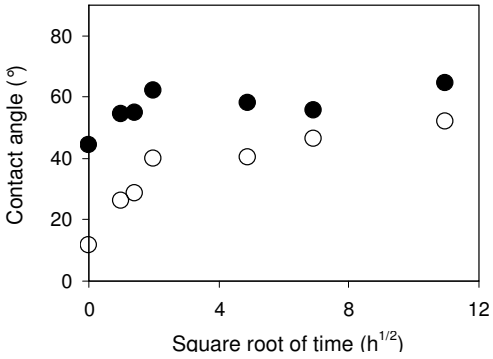

Fig. 10. Contact angle measurements as a function of incubation time in ambient atmosphere performed on (●) native stainless steel and (○) after UV-ozone treatment.

It must be emphasized that outgassing a material of high surface energy is not suitable to prevent adventitious contamination of the surface. Materials cleaned with UV-ozone treatment and showing a water contact angle below 5° reached an appreciable contact angle (20° for silica, 40° for stainless steel and gold) after a stay of 5 minutes in the vacuum of the spectrometer chamber. The high rate of contamination may be due to evacuation itself, owing to the increased proportion of organic compounds in the residual gas and to their increased rate of transfer (Caillou et al., 2008).

4.4. Thickness of the organic adlayer

No variation of the relative concentrations of organic compounds was revealed by angle-resolved XPS analysis (Figure 4) but an effect of stratification may be masked by the surface roughness. The evaluation of the adlayer thickness may clarify whether the increase of the silane or protein concentration resulting from the respective treatments reflects an addition of or a substitution by new compounds in the adlayer.

If the surface is considered as atomically smooth and the organic layer is continuous with a constant thickness, the apparent concentration ratio [*C*]/[*Cr*] may be computed using the following equation:

$$\frac{[C]}{[Cr]} = \frac{i_{Cr}}{i_C}\frac{\sigma_C}{\sigma_{Cr}}\frac{\lambda_C^{Org} C_C^{Org}\left[1-\exp\left(\frac{-t}{\lambda_C^{Org}\cos\theta}\right)\right]}{\lambda_{Cr}^{Ox} C_{Cr}^{Ox}\exp\left(\frac{-t}{\lambda_{Cr}^{Org}\cos\theta}\right)} \quad (8)$$

i_C and i_{Cr} are the relative sensitivity factors of C and Cr, respectively, provided by the spectrometer manufacturer. The photoionization cross sections σ are 1 for C 1s and 11.7 for Cr 2p (Scofield, 1976). The superscripts Org and Ox designate the organic adlayer and the passive oxide layer, respectively. The concentration of Cr in the oxide layer (C_{Cr}^{Org} ; between 0.015 and 0.020 mol.cm^{-3}, depending on the sample), was determined on the basis of the above discussion indicating that the oxide layer is constituted with FeOOH, CrOOH, $Ni(OH)_2$ and MoO_3 (*section 4.1*). Note that this is in agreement with a concentration of inorganic oxygen close to ($O_{tot} - O_{org}$), owing to the low concentration of silane. The concentration of carbon in the organic adlayer was determined on the basis of the surface composition modeled as detailed above, using the densities given in Table 3. The density of silane, was taken as the average between the densities of 3-aminopropyl(trimethylsilane) (0.8 g.cm^{-3}) and 3-aminopropyl(trimethoxysilane) (1.0 g.cm^{-3}). The electron inelastic mean free paths (IMFP) were calculated using the Quases program (http://www.quases.com) and the TPP2M formula (Tanuma et al., 1997), considering the matrix composition deduced above. For λ_{Cr}^{Ox}, values of 2.04 and 1.99 nm were computed for FeOOH and CrOOH, respectively (energy gap 2.3 and 1.6 eV, respectively). Considering an energy gap of 6 eV for the organic compounds, respective values of λ_C^{Org} and λ_{Cr}^{Org} were 3.79 and 3.04 nm in hydrocarbon-like compounds [$(CH_2)_n$], 3.59 nm and 2.89 nm in protein, 3.67 and 2.00 nm in polysaccharides [$(C_6(H_2O)_5)_n$], and 3.68 and 2.95 nm in silane [$H_2N(CH_2)_3SiO_{1.5}$].

The thickness of the organic adlayer deduced for photoelectron collection angles θ = 0° and 60° is given in Table 4. The difference between the values computed for the two

photoelectron collection angles is due to the approximation of a smooth surface while the analyzed surface is rough at the scale of the inelastic mean free paths. The real organic adlayer thickness should be between the values given in Table 4. Comparison between nat and sil samples suggests that silane just adds up to the contaminants. A 3.0 nm thick adlayer containing 25 wt.% silane corresponds to 4.5 molecules.nm^{-2}. This value is consistent with a monolayer of silane, however the retained silane is mixed with a much larger amount of contaminants. The protein treatment of silanized substrates (compare sil+Gox and sil+BS+Gox to sil) led to a significant decrease of the amount of hydrocarbon-like compounds, while the adlayer thickness did not change appreciably. This suggests that the protein adsorption caused the displacement of part of contamination present on the silanized stainless steel surface in the form of hydrocarbon-like compounds.

5. Conclusion

The decomposition of the C 1s and O 1s peak provided a distinct evaluation of oxygen present in inorganic oxide, inorganic hydroxide and organic compounds. This led to a stoichiometry close to (Fe, Cr)OOH for iron and chromium species in the passive layer. The elemental composition of the organic adlayer was converted into concentration of model organic compounds: protein, silane and contaminants. For the latter, extreme poles of hydrocarbons and polysaccharides were taken as models.

Silanization increased markedly the retention of glucose oxidase, whether or not using a linker expected to couple the enzyme with the silane. Direct retention of the enzyme by the silane may be attributed to electrostatic attractions with the protonated amine groups (Jasienak et al., 2009). It is thus demonstrated, with the same biomolecule, that its retention by using an APTES-treated substrate and a linker does not infer covalent grafting through the linker. The occurrence of covalent binding might possibly be evaluated by examining the retention upon aging in electrolytes, keeping in mind that the silane layer itself may alter in these conditions (Dekeyser et al., 2008).

The thickness of the organic adlayer was of the order of 3 nm. In all cases, the concentration of contaminants exceeded the concentration of silane and protein. Angle-resolved measurements did not reveal any stratification in the organic adlayer, but this was not conclusive since the effect of a stratification may be masked owing to the roughness created by nanoparticles of inorganic oxyhydroxide present at the stainless steel surface. The presence of organic contaminants is unavoidable when high energy materials are exposed to air for a few hours or to vacuum for a very short time. However the influence of contaminants on the desired surface reactions is not known and is difficult to establish. The best to reduce contamination is to thoroughly clean the substrate by oxidation, to minimize the time of contact of substrates with air at any stage, and to strictly avoid outgassing. Water contact angle measurement is the best way to assess the cleanliness of the native substrate but the information will not be unambiguous after silanization and further treatments.

6. Acknowledgments

The authors thank Simon Degand for his help in statistics. They acknowledge the support of the "Conseil Régional de Picardie" (France) and the National Fondation for Scientific Research (F.N.R.S. – Belgium).

7. References

Ahimou, F., Boonaert, C.J.P., Adriaensen, Y., Jacques, P., Thonart, P., Paquot, M. & Rouxhet, P.G. (2007) XPS analysis of chemical functions at the surface of Bacillus subtilis, *Journal of Colloid and Interface Science*,Vol. 309, No. 1, pp. 49-55.

Asenath Smith, E. & Chen, W. (2008) How To Prevent the Loss of Surface Functionality Derived from Aminosilanes, *Langmuir*,Vol. 24, No. 21, pp. 12405-12409.

Balasundaram, G., Sato, M. & Webster, T.J. (2006) Using hydroxyapatite nanoparticles and decreased crystallinity to promote osteoblast adhesion similar to functionalizing with RGD, *Biomaterials*,Vol. 27, No. 14, pp. 2798-2805.

Bartouilh de Taillac, L., Porté-Durrieu, M.C., Labrugère, C., Bareille, R., Amédée, J. & Baquey, C. (2004) Grafting of RGD peptides to cellulose to enhance human osteoprogenitor cells adhesion and proliferation, *Composites Science and Technology*, Vol. 64, No. 6, pp. 827-837.

Boucher, C., Liberelle, B.t., Jolicoeur, M., Durocher, Y. & De Crescenzo, G. (2009) Epidermal growth factor tethered through coiled-coil interactions induces cell surface receptor phosphorylation, *Bioconjugate Chemistry*, Vol. 20, No. 8, pp. 1569-1577.

Briggs, D. & Seah, M.P. (1990) *Practical Surface Analysis, Auger and X-ray Photoelectron Spectroscopy* (Chichester, UK, Wiley).

Caillou, S., Gerin, P.A., Nonckreman, C.J., Fleith, S., Dupont-Gillain, C.C., Landoulsi, J., Pancera, S.M., Genet, M.J. & Rouxhet, P.G. (2008) Enzymes at solid surfaces: Nature of the interfaces and physico-chemical processes, *Electrochimica Acta*, Vol. 54, No. 1, pp. 116-122.

Charbonneau, C., Liberelle, B., Hébert, M.-J., De Crescenzo, G. & Lerouge, S. (2011) Stimulation of cell growth and resistance to apoptosis in vascular smooth muscle cells on a chondroitin sulfate/epidermal growth factor coating, *Biomaterials*, Vol. 32, No. 6, pp. 1591-1600.

Cho, Y. & Ivanisevic, A. (2004) SiOx Surfaces with lithographic features composed of a TAT peptide, *The Journal of Physical Chemistry B*, Vol. 108, No. 39, pp. 15223-15228.

Chuang, Y.-J., Huang, J.-W., Makamba, H., Tsai, M.-L., Li, C.-W. & Chen, S.-H. (2006) Electrophoretic mobility shift assay on poly(ethylene glycol)-modified glass microchips for the study of estrogen responsive element binding, *Electrophoresis*, Vol. 27, No. 21, pp. 4158-4165.

Davis, D.H., Giannoulis, C.S., Johnson, R.W. & Desai, T.A. (2002) Immobilization of RGD to <1 1 1> silicon surfaces for enhanced cell adhesion and proliferation, *Biomaterials*, Vol. 23, No. 19, pp. 4019-4027.

Dekeyser, C.M., Buron, C.C., Mc Evoy, K., Dupont-Gillain, C.C., Marchand-Brynaert, J., Jonas, A.M. & Rouxhet, P.G. (2008) Oligo(ethylene glycol) monolayers by silanization of silicon wafers: Real nature and stability, *Journal of Colloid and Interface Science*, Vol. 324, No. 1-2, pp. 118-126.

Doh, J. & Irvine, D.J. (2006) Immunological synapse arrays: Patterned protein surfaces that modulate immunological synapse structure formation in T cells, *Proceedings of the National Academy of Sciences*, Vol. 103, No. 15, pp. 5700-5705.

Dufrêne, Y.F. & Rouxhet, P.G. (1996) Surface composition, surface properties, and adhesiveness of Azospirillum brasilense - variation during growth, *Canadian Journal of Microbiology*, Vol. 42, pp. 548-556.

Dupont, I., Féron, D. & Novel, G. (1998) Effect of glucose oxidase activity on corrosion potential of stainless steels in seawater, *International Biodeterioration & Biodegradation*, Vol. 41, No. 1, pp. 13-18.

El-Ghannam, A.R., Ducheyne, P., Risbud, M., Adams, C.S., Shapiro, I.M., Castner, D., Golledge, S. & Composto, R.J. (2004) Model surfaces engineered with nanoscale roughness and RGD tripeptides promote osteoblast activity, *Journal of Biomedical Materials Research Part A*, Vol. 68A, No. 4, pp. 615-627.

Genet, M.J., Dupont-Gillain, C.C. & Rouxhet, P.G. (2008) XPS analysis of biosystems and biomaterials, in: M. E. (Ed) *Medical Applications of Colloids* (New York, Springer), pp. 177-307.

Gooding, J.J. & Ciampi, S. (2011) The molecular level modification of surfaces: from self-assembled monolayers to complex molecular assemblies, *Chemical Society Reviews*, DOI: 10.1039/c0cs00139b.

Haensch, C., Hoeppener, S. & Schubert, U.S. (2010) Chemical modification of self-assembled silane based monolayers by surface reactions, *Chemical Society Reviews*, Vol. 39, No. 6, pp. 2323-2334.

Hanawa T. 2002. Metallic biomaterials. In: Ikada Y, editor. Recent research and developments in biomaterials, Research Signpost, p. 11-31.

Howarter, J.A. & Youngblood, J.P. (2006) Optimization of silica silanization by 3-Aminopropyltriethoxysilane, *Langmuir*, Vol. 22, No. 26, pp. 11142-11147.

Iucci, G., Dettin, M., Battocchio, C., Gambaretto, R., Bello, C.D. & Polzonetti, G. (2007) Novel immobilizations of an adhesion peptide on the TiO2 surface: An XPS investigation, *Materials Science and Engineering: C*, Vol. 27, No. 5-8, pp. 1201-1206.

Jasienak, M., Suzuki, S., Montero, M., Wentrup-Byrne, E., Griesser, H.J. & Grondahl, L. (2009) Time-of-flight secondary ion mass spectrometry study of the orientation of a bifunctional diblock copolymer attached to a solid substrate, *Langmuir*, Vol. 25, No. 2, pp. 1011-1019.

Jin, L., Horgan, A. & Levicky, R. (2003) Preparation of end-tethered DNA monolayers on siliceous surfaces using heterobifunctional cross-linkers, *Langmuir*, Vol. 19, No. 17, pp. 6968-6975.

Katsikogianni, M.G. & Missirlis, Y.F. (2010) Interactions of bacteria with specific biomaterial surface chemistries under flow conditions, *Acta Biomaterialia*, Vol. 6, No. 3, pp. 1107-1118.

Killian, M.S., Wagener, V., Schmuki, P. & Virtanen, S. (2010) Functionalization of metallic magnesium with protein layers via linker molecules, *Langmuir*, Vol. 26, No. 14, pp. 12044-12048.

Kim, J., Cho, J., Seidler, P.M., Kurland, N.E. & Yadavalli, V.K. (2010) Investigations of chemical modifications of amino-terminated organic films on silicon substrates and controlled protein immobilization, *Langmuir*, Vol. 26, No. 4, pp. 2599-2608.

Kim, J., Seidler, P., Wan, L.S. & Fill, C. (2009a) Formation, structure, and reactivity of amino-terminated organic films on silicon substrates, *Journal of Colloid and Interface Science*, Vol. 329, No. 1, pp. 114-119.

Kim, W.-J., Kim, S., Lee, B.S., Kim, A., Ah, C.S., Huh, C., Sung, G.Y. & Yun, W.S. (2009b) Enhanced protein immobilization efficiency on a TiO2 surface modified with a hydroxyl functional group, *Langmuir*, Vol. 25, No. 19, pp. 11692-11697.

Koh, I., Wang, X., Varughese, B., Isaacs, L., Ehrman, S.H. & English, D.S. (2006) Magnetic iron oxide nanoparticles for biorecognition: Evaluation of surface coverage and activity, *The Journal of Physical Chemistry B*, Vol. 110, No. 4, pp. 1553-1558.

Kohli, P., Taylor, K.K., Harris, J.J. & Blanchard, G.J. (1998) Assembly of covalently-coupled disulfide multilayers on gold, *Journal of the American Chemical Society*, Vol. 120, No. 46, pp. 11962-11968.

Landoulsi, J., Dagbert, C., Richard, C., Sabot, R., Jeannin, M., El Kirat, K. & Pulvin, S. (2009) Enzyme-induced ennoblement of AISI 316L stainless steel: Focus on pitting corrosion behavior, *Electrochimica Acta*, Vol. 54, No. 28, pp. 7401-7406.

Landoulsi, J., Genet, M.J., Richard, C., El Kirat, K., Pulvin, S. & Rouxhet, P.G. (2008a) Evolution of the passive film and organic constituents at the surface of stainless steel immersed in fresh water, *Journal of Colloid and Interface Science*, Vol. 318, No. 2, pp. 278-289.

Landoulsi, J., Genet, M.J., Richard, C., El Kirat, K., Rouxhet, P.G. & Pulvin, S. (2008b) Ennoblement of stainless steel in the presence of glucose oxidase: Nature and role of interfacial processes, *Journal of Colloid and Interface Science*, Vol. 320, No. 2, pp. 508-519.

Landoulsi, J., Kirat, K.E., Richard, C., Féron, D. & Pulvin, S. (2008c) Enzymatic approach in microbial-influenced corrosion: A review based on Stainless Steels in Natural Waters, *Environmental Science & Technology*, Vol. 42, No. 7, pp. 2233-2242.

Lapin, N.A. & Chabal, Y.J. (2009) Infrared characterization of biotinylated silicon oxide surfaces, surface stability, and specific attachment of streptavidin, *The Journal of Physical Chemistry B*, Vol. 113, No. 25, pp. 8776-8783.

Le Bozec, N., Compère, C., L'Her, M., Laouenan, A., Costa, D. & Marcus, P. (2001) Influence of stainless steel surface treatment on the oxygen reduction reaction in seawater, *Corrosion Science*, Vol. 43, No. 4, pp. 765-786.

Li, G., Yang, P., Qin, W., Maitz, M.F., Zhou, S. & Huang, N. (2011) The effect of coimmobilizing heparin and fibronectin on titanium on hemocompatibility and endothelialization, *Biomaterials*, Vol. 32, No. 21, pp. 4691-4703.

Libertino, S., Giannazzo, F., Aiello, V., Scandurra, A., Sinatra, F., Renis, M. & Fichera, M. (2008) XPS and AFM characterization of the enzyme glucose oxidase immobilized on SiO_2 surfaces, *Langmuir*, Vol. 24, No. 5, pp. 1965-1972.

Ma, L., Zhou, J., Gao, C. & Shen, J. (2007) Incorporation of basic fibroblast growth factor by a layer-by-layer assembly technique to produce bioactive substrates, *Journal of Biomedical Materials Research Part B: Applied Biomaterials*, Vol. 83B, No. 1, pp. 285-292.

Mantel, M., Rabinovich, Y.I., Wightman, J.P. & Yoon, R.H. (1995) A Study of Hydrophobic Interactions between Stainless Steel and Silanated Glass Surface Using Atomic Force Microscopy, *Journal of Colloid and Interface Science*, Vol. 170, No. 1, pp. 203-214.

Martin, H.J., Schulz, K.H., Bumgardner, J.D. & Walters, K.B. (2007) XPS Study on the Use of 3-Aminopropyltriethoxysilane to Bond Chitosan to a Titanium Surface, *Langmuir*, Vol. 23, No. 12, pp. 6645-6651.

Matinlinna, J., P., Lassila, L., V. J., Özcan, M., Yli-Urpo, A. & Vallittu, P., K. (2004) An introduction to silanes and their clinical applications in dentistry, *International Journal of Prosthodontics*, Vol. 17, No. 211, pp. 155-164.

Matinlinna, J.P. & Vallittu, P.K. (2007) Silane based concepts on bonding resin composite to metals, *The Journal of Contemporary Dental Practice*, Vol. 8, No. 2, pp. 1-8.

Meng, S., Liu, Z., Shen, L., Guo, Z., Chou, L.L., Zhong, W., Du, Q. & Ge, J. (2009) The effect of a layer-by-layer chitosan-heparin coating on the endothelialization and coagulation properties of a coronary stent system, *Biomaterials*, Vol. 30, No. 12, pp. 2276-2283.

Minier, M., Salmain, M.l., Yacoubi, N., Barbes, L., Méthivier, C., Zanna, S. & Pradier, C.-M. (2005) Covalent Immobilization of Lysozyme on Stainless Steel. Interface spectroscopic characterization and measurement of enzymatic activity, *Langmuir*,Vol. 21, No. 13, pp. 5957-5965.

Mosse, W.K.J., Koppens, M.L., Gengenbach, T.R., Scanlon, D.B., Gras, S.L. & Ducker, W.A. (2009) Peptides grafted from solids for the control of interfacial properties, *Langmuir*, Vol. 25, No. 3, pp. 1488-1494.

Müller, R., Abke, J., Schnell, E., Macionczyk, F., Gbureck, U., Mehrl, R., Ruszczak, Z., Kujat, R., Englert, C., Nerlich, M. & Angele, P. (2005) Surface engineering of stainless steel materials by covalent collagen immobilization to improve implant biocompatibility, *Biomaterials*, Vol. 26, No. 34, pp. 6962-6972.

Nanci, A., Wuest, J.D., Peru, L., Brunet, P., Sharma, V., Zalzal, S. & McKee, M.D. (1998) Chemical modification of titanium surfaces for covalent attachment of biological molecules, *Journal of Biomedical Materials Research*, Vol. 40, No. 2, pp. 324-335.

NIST X-ray Photoelectron Spectroscopy Database, NIST Standard Reference Database 20, Version 3.4 (Web Version), http://srdata.nist.gov/xps/index.htm.

North, S.H., Lock, E.H., Cooper, C.J., Franek, J.B., Taitt, C.R. & Walton, S.G. (2004) Plasma-based surface modification of polystyrene microtiter plates for covalent immobilization of biomolecules, *ACS Applied Materials & Interfaces*, Vol. 2, No. 10, pp. 2884-2891.

Olefjord, I. & Wegrelius, L. (1996) The influence of nitrogen on the passivation of stainless steels, *Corrosion Science*, Vol. 38, No. 7, pp. 1203-1220.

Palestino, G., Agarwal, V., Aulombard, R., PeÌ rez, E.a. & Gergely, C. (2008) Biosensing and protein fluorescence enhancement by functionalized porous silicon devices, *Langmuir*, Vol. 24, No. 23, pp. 13765-13771.

Pasternack, R.M., Rivillon Amy, S. & Chabal, Y.J. (2008) Attachment of 3-(Aminopropyl)triethoxysilane on silicon oxide surfaces: Dependence on solution temperature, *Langmuir*, Vol. 24, No. 22, pp. 12963-12971.

Plueddemann, E.W. (1991) *Silane Coupling Agents* (New York, Plenum).

Porté-Durrieu, M.C., Guillemot, F., Pallu, S., Labrugère, C., Brouillaud, B., Bareille, R., Amédée, J., Barthe, N., Dard, M. & Baquey, C. (2004) Cyclo-(DfKRG) peptide grafting onto Ti-6Al-4V: physical characterization and interest towards human osteoprogenitor cells adhesion, *Biomaterials*, Vol. 25, No. 19, pp. 4837-4846.

Puleo, D.A. (1997) Retention of enzymatic activity immobilized on silanized Co-Cr-Mo and Ti-6Al-4V, *Journal of Biomedical Materials Research*, Vol. 37, pp. 222-228.

Quan, D., Kim, Y. & Shin, W. (2004) Characterization of an amperometric laccase electrode covalently immobilized on platinum surface, *Journal of Electroanalytical Chemistry*, Vol. 561, pp. 181-189.

Ratner B.D., Hoffman A.S., Schoen F.J. & Lemons J.E. (Eds) (2004) *Biomaterials Science: An Introduction to Materials in Medecine* (Academic Press, San Diego, U.S.A., 2d Ed.).

Rouxhet, P.G. & Genet, M.J. (2011) XPS analysis of bio-organic systems, *Surface and Interface Analysis*. (In press).

Rouxhet, P.G., Misselyn-Bauduin, A.M., Ahimou, F., Genet, M.J., Adriaensen, Y., Desille, T., Bodson, P. & Deroanne, C. (2008) XPS analysis of food products: toward chemical functions and molecular compounds, *Surface and Interface Analysis*,Vol. 40, No. 3-4, pp. 718-724.

Sarath Babu, V.R., Kumar, M.A., Karanth, N.G. & Thakur, M.S. (2004) Stabilization of immobilized glucose oxidase against thermal inactivation by silanization for biosensor applications, *Biosensors and Bioelectronics*,Vol. 19, No. 10, pp. 1337-1341.

Sargeant, T.D., Rao, M.S., Koh, C.-Y. & Stupp, S.I. (2008) Covalent functionalization of NiTi surfaces with bioactive peptide amphiphile nanofibers, *Biomaterials*,Vol. 29, No. 8, pp. 1085-1098.

Sasou, M., Sugiyama, S., Yoshino, T. & Ohtani, T. (2003) Molecular flat mica surface silanized with methyltrimethoxysilane for fixing and straightening DNA, *Langmuir*, Vol. 19, No. 23, pp. 9845-9849.

Schuessele, A., Mayr, H., Tessmar, J. & Goepferich, A. (2009) Enhanced bone morphogenetic protein-2 performance on hydroxyapatite ceramic surfaces, *Journal of Biomedical Materials Research Part A*, Vol. 90A, No. 4, pp. 959-971.

Scofield, J.H. (1976) Hartree-Slater subshell photoionization cross-sections at 1254 and 1487 eV, *Journal of Electron Spectroscopy and Related Phenomena*, Vol. 8, No. 2, pp. 129-137.

Siperko, L.M., Jacquet, R. & Landis, W.J. (2006) Modified aminosilane substrates to evaluate osteoblast attachment, growth, and gene expression in vitro, *Journal of Biomedical Materials Research Part A*, Vol. 78A, No. 4, pp. 808-822.

Son, K.J., Ahn, S.H., Kim, J.H. & Koh, W.-G. (2011) Graft copolymer-templated mesoporous TiO_2 films micropatterned with Poly(ethylene glycol) hydrogel: Novel platform for highly sensitive protein microarrays, *ACS Applied Materials & Interfaces*,Vol. 3, No. 2, pp. 573-581.

Sordel, T., Kermarec-Marcel, F., Garnier-Raveaud, S., Glade, N., Sauter-Starace, F., Pudda, C., Borella, M., Plissonnier, M., Chatelain, F., Bruckert, F. & Picollet-D'hahan, N. (2007) Influence of glass and polymer coatings on CHO cell morphology and adhesion, *Biomaterials*,Vol. 28, No. 8, pp. 1572-1584.

Subramanian, A., Kennel, S.J., Oden, P.I., Jacobson, K.B., Woodward, J. & Doktycz, M.J. (1999) Comparison of techniques for enzyme immobilization on silicon supports, *Enzyme and Microbial Technology*,Vol. 24, No. 1-2, pp. 26-34.

Suzuki, N. & Ishida, H. (1996) A review on the structure and characterization techniques of silane/matrix interphases, *Macromolecular Symposia*,Vol. 108, No. 1, pp. 19-53.

Suzuki, S., Whittaker, M.R., Grøndahl, L., Monteiro, M.J. & Wentrup-Byrne, E. (2006) Synthesis of soluble phosphate polymers by RAFT and their in vitro mineralization, *Biomacromolecules,* Vol. 7, No. 11, pp. 3178-3187.

Tanuma, S., Powell, C.J. & Penn, D.R. (1997) Calculations of electron inelastic mean free paths (IMFPs) VI. Analysis of the gries inelastic scattering model and predictive IMFP equation, *Surface and Interface Analysis*, Vol. 25, No. 1, pp. 25-35.

Tesson, B., Genet, M.J., Fernandez, V., Degand, S., Rouxhet, P.G. & Martin-Jézéquel, V. (2009) Surface chemical composition of diatoms, *ChemBioChem*, Vol. 10, No. 12, pp. 2011-2024.

Toworfe, G.K., Bhattacharyya, S., Composto, R.J., Adams, C.S., Shapiro, I.M. & Ducheyne, P. (2009) Effect of functional end groups of silane self-assembled monolayer surfaces on apatite formation, fibronectin adsorption and osteoblast cell function, *Journal of Tissue Engineering and Regenerative Medicine*, Vol. 3, No. 1, pp. 26-36.

Toworfe, G.K., Composto, R.J., Shapiro, I.M. & Ducheyne, P. (2006) Nucleation and growth of calcium phosphate on amine-, carboxyl- and hydroxyl-silane self-assembled monolayers, *Biomaterials*, Vol. 27, No. 4, pp. 631-642.

Vaidya, A.A. & Norton, M.L. (2004) DNA attachment chemistry at the flexible silicone elastomer surface: Toward disposable microarrays, *Langmuir*, Vol. 20, No. 25, pp. 11100-11107.

Weetall, H.H. (1993) Preparation of immobilized proteins covalently coupled through silane coupling agents to inorganic supports. *Applied Biochemistry and Biotechnology*, Vol. 41, No. 157, pp. 157-188.

Weng, Y.J., Hou, R.X., Li, G.C., Wang, J., Huang, N. & Liu, H.Q. (2008) Immobilization of bovine serum albumin on TiO_2 film via chemisorption of H_3PO_4 interface and effects on platelets adhesion, *Applied Surface Science*, Vol. 254, No. 9, pp. 2712-2719.

Williams, R. (2010) *Surface Modifications of Biomaterials: Methods Analysis and Applications (*Woodhead Publishing Ltd).

Wink, T., van Zuilen, S.J., Bult, A. & van Bennekom, W.P. (1997) Self-assembled monolayers for biosensors. *Analyst*, Vol 122, pp. 43R-50R

Xiao, S.J., Textor, M., Spencer, N.D., Wieland, M., Keller, B. & Sigrist, H. (1997) Immobilization of the cell-adhesive peptide Arg–Gly–Asp–Cys (RGDC) on titanium surfaces by covalent chemical attachment, *Journal of Materials Science: Materials in Medicine*, Vol. 8, No. 12, pp. 867-872.

Xie, Y., Hill, C.A.S., Xiao, Z., Militz, H. & Mai, C. (2010) Silane coupling agents used for natural fiber/polymer composites: A review, *Composites Part A: Applied Science and Manufacturing*, Vol. 41, No. 7, pp. 806-819.

Yoshioka, T., Tsuru, K., Hayakawa, S. & Osaka, A. (2003) Preparation of alginic acid layers on stainless-steel substrates for biomedical applications, *Biomaterials*, Vol. 24, No. 17, pp. 2889-2894.

Zhou, G.-T., Yao, Q.-Z., Wang, X. & Yu, J.C. (2006) Preparation and characterization of nanoplatelets of nickel hydroxide and nickel oxide, *Materials Chemistry and Physics*, Vol. 98, No. 2-3, pp. 267-272.

Zile, M.A., Puckett, S. & Webster, T.J. Nanostructured titanium promotes keratinocyte density, *Journal of Biomedical Materials Research Part A*, Vol. 97A, No. 1, pp. 59-65.

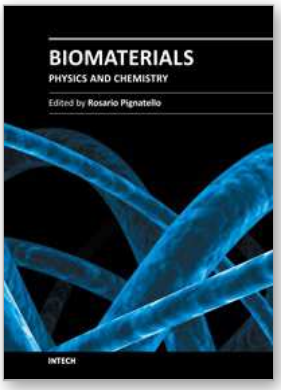

Biomaterials - Physics and Chemistry

Edited by Prof. Rosario Pignatello

ISBN 978-953-307-418-4
Hard cover, 490 pages
Publisher InTech
Published online 14, November, 2011
Published in print edition November, 2011

These contribution books collect reviews and original articles from eminent experts working in the interdisciplinary arena of biomaterial development and use. From their direct and recent experience, the readers can achieve a wide vision on the new and ongoing potentialities of different synthetic and engineered biomaterials. Contributions were selected not based on a direct market or clinical interest, but based on results coming from very fundamental studies. This too will allow to gain a more general view of what and how the various biomaterials can do and work for, along with the methodologies necessary to design, develop and characterize them, without the restrictions necessarily imposed by industrial or profit concerns. The chapters have been arranged to give readers an organized view of this research area. In particular, this book contains 25 chapters related to recent researches on new and known materials, with a particular attention to their physical, mechanical and chemical characterization, along with biocompatibility and hystopathological studies. Readers will be guided inside the range of disciplines and design methodologies used to develope biomaterials possessing the physical and biological properties needed for specific medical and clinical applications.

How to reference

In order to correctly reference this scholarly work, feel free to copy and paste the following:

Jessem Landoulsi, Michel J. Genet, Karim El Kirat, Caroline Richard, Sylviane Pulvin and Paul G. Rouxhet (2011). Silanization with APTES for Controlling the Interactions Between Stainless Steel and Biocomponents: Reality vs Expectation, Biomaterials - Physics and Chemistry, Prof. Rosario Pignatello (Ed.), ISBN: 978-953-307-418-4, InTech, Available from: http://www.intechopen.com/books/biomaterials-physics-and-chemistry/silanization-with-aptes-for-controlling-the-interactions-between-stainless-steel-and-biocomponents-r

INTECH
open science | open minds

InTech Europe
University Campus STeP Ri
Slavka Krautzeka 83/A
51000 Rijeka, Croatia
Phone: +385 (51) 770 447
Fax: +385 (51) 686 166
www.intechopen.com

InTech China
Unit 405, Office Block, Hotel Equatorial Shanghai
No.65, Yan An Road (West), Shanghai, 200040, China
中国上海市延安西路65号上海国际贵都大饭店办公楼405单元
Phone: +86-21-62489820
Fax: +86-21-62489821